Available online at www.sciencedirect.com

jmr&t Journal of Materials Research and Technology

journal homepage: www.elsevier.com/locate/jmrt

Original Article

Impact of Ni on the thermophysical and thermodynamic properties of Fe–C–Ni based alloys

Ľubomíra Drozdová[*], *Bedřich Smetana, Mario Machů, Vlastimil Novák, Jiřina Vontorová, Simona Zlá, Monika Kawuloková, Lenka Řeháčková, Svetlana Sorokina*

Faculty of Materials Science and Technology, VŠB-Technical University of Ostrava, 17. listopadu 2172/15, 708 00 Ostrava-Poruba, EU, Czech Republic

ARTICLE INFO

Article history:
Received 1 July 2022
Accepted 29 August 2022
Available online 6 September 2022

Keywords:
Fe-C-Ni alloys
Phase transition temperatures
Heat capacity
Enthalpy change
Heat of fusion
Coefficient of thermal expansion

ABSTRACT

Three model alloys based on Fe-C-Ni were studied containing carbon between 0.338 and 0.382 wt. % and nickel between 1.084 and 4.478 wt. %. Phase transition temperatures, heat capacity, enthalpy change, heat of fusion, coefficient of thermal expansion, and density were experimentally and theoretically determined in the high-temperature area from 1000 °C to 1595 °C. A number of techniques, namely differential thermal analysis (DTA), differential scanning calorimetry (DSC), and dilatometry, were used in this study, and the heat of fusion was determined by two approaches, that is, from the DSC peak area and from the enthalpy change. The experimental data were compared and discussed with the calculation results obtained using SW IDS, JMatPro, and Thermo-Calc operating with the commercially available TCFE8 thermodynamic database. The obtained experimental results show that the liquidus temperature and the coefficient of thermal expansion decrease with increasing nickel content. On the contrary, the density and heat of fusion values derived from the DSC peak increase with increasing nickel content. Furthermore, an ambiguous influence of nickel on the change in solidus temperature, heat capacity, enthalpy change, and heat of fusion obtained from the enthalpy change was observed.

1. Introduction

Iron-based alloys are of great practical importance because they have technical properties that allow their wide use in the construction, energy, machinery, automotive, and consumer industries [1–3]. These materials are in demand not only for their excellent technical properties and relative affordability compared to other metal alloys or technical materials but also for their high recycling potential [4], which is very important in today's world, where sustainability is a crucial aspect of the future [5], as efforts to increase the prosperity of humanity

* Corresponding author.
E-mail address: lubomira.drozdova@vsb.cz (Ľ. Drozdová).
https://doi.org/10.1016/j.jmrt.2022.08.159

will go hand in hand with the need to reduce the energy and environmental demands of civilization [6,7].

The large variability of the chemical composition of ferrous alloys, e.g., steels, which represent an example of a multicomponent alloy, causes a lack of experimental thermophysical and thermodynamic data for each alloy [8]. Accurate data is needed for proper use in a specific application and in the process of producing semi-finished and finished products from a particular steel grade, as final properties depend not only on the chemical composition but also on the processes of casting, forming, heat, or surface treatment, machining, welding, etc. [9,10]. Furthermore, the experimental data are applicable to simulations as they represent a cheaper alternative to experiments on actual manufacturing devices (blast furnace operation, secondary steel treatment, continuous casting machines, rolling mills, or forging machines).

The results obtained highly depend on the quality of the input data, so adequate experimental data on solidus and liquidus and other phase change temperatures, heat capacities, heat of fusion, enthalpy, and coefficient of thermal expansion is required [11].

In general, there are two basic approaches to determining material properties. The primary option is the experimental measurement, which provides the most valuable data but may be burdened by measurement error. The material properties mentioned above, such as phase transformation temperatures and specific heat capacities, heat of fusion, or coefficients of thermal expansion in both the low and high-temperature range, can be measured using thermal analysis methods [12,13].

Phase change temperatures (liquidus, solidus and peritectic temperatures) are most often measured by means of differential scanning calorimetry (DSC), differential thermal analysis (DTA), or dilatometry, sometimes complemented with high-temperature laser scanning confocal microscopy (HT- LSCM) [14–16].

Due to the time and cost requirements of high-temperature measurements, SW modeling is often used based on data obtained from a limited number of measurements on a limited number of alloys. Software based on the thermodynamic databases CALPHAD, built, for example, into Computherm, Thermo-Calc, Fact-Sage or Pandat, is often used [17,18].

The development of CALPHAD-based thermodynamic databases of multicomponent systems consists of combining simple binary, and ternary systems into more complex systems [19–21].

Nickel is one of the austenite-forming elements that completely open the γ region. These elements expand the austenite stability region by lowering the transformation end temperature $\alpha \rightarrow \gamma$ ($T_{\alpha\rightarrow\gamma,E}$) and increasing the peritectic transformation temperature (T_P). In the Fe–C–Ni ternary system, nickel does not form a separate carbide, so it is completely dissolved in the basic matrix. Nickel increases the strength of ferrite more than chromium. Increases hardenability, but significantly less than chromium. It is also used to increase toughness at low temperatures. Austenite-forming steels are characterized by a higher thermal expansion and a lower coefficient of thermal conductivity. They show higher resistance to corrosion cracking and intergranular corrosion [22–24]. Nickel is mainly used in steels with high toughness, especially at negative temperatures. High nickel steels have an austenitic nonmagnetic structure [22]. Nickel is always combined with other alloying elements in steels to obtain maximum mechanical properties. Nickel steels have a low or medium C content of up to 0.5 wt. %, because with higher content, the content of residual austenite increases in the matrix after quenching. Chromium-nickel steels have good hardenability and toughness. They contain chromium from 0.5 to 1.2 wt. % and nickel from 1.2 to 5.2 wt. %.

This paper focuses on the study of phase transition temperatures, heat capacity, enthalpy change, heat of fusion, coefficient of thermal expansion, and density in the high-temperature area. Three model alloys based on Fe–C–Ni were studied. Experimental results were obtained using differential thermal analysis (DTA), differential scanning calorimetry (DSC), and dilatometry. The experimentally obtained results were discussed with the results calculated using IDS, JMatPro, and Thermo-Calc software. This work deals with the influence of the nickel content on the change in the experimentally and theoretically obtained results.

Obtaining experimental results in the high-temperature region, especially in the melt, is very challenging experimentally. The experimental results obtained are often influenced by many factors. The results affect the interactions associated with the melting process, chemical heterogeneity, and stabilization of experimental conditions, which is very difficult at high temperatures. This work provides a comprehensive study of the impact of nickel on selected thermophysical properties of Fe-C-Ni-based alloys in this area.

2. Theoretical calculations

As experimental measurements are time and money-consuming, empirical and semi-empirical tools were developed based on previous experimental works. Development went from simple linear functions of composition to specialized software working with different methods, e.g., phase-field method, CALPHAD method, or semi-empirical method.

SW InterDendriticSolidification (IDS) is a thermodynamic-kinetic-empirical tool to simulate segregation and solidification phenomena, including phase transformations from melt to room temperature of low-alloy steels and stainless steels with a chromium content of up to 26 mass% [25]. The results obtained in this work were calculated in SW IDS version 1.3.1. All elements were included in the calculations.

SW JMatPro (JMP) is a simulation software that calculates a wide range of material properties of alloys, focusing mainly on multicomponent alloys used in industrial practice [26]. The results presented in this work were obtained by SW JMatPro version 11.1 and the General Steel database. In the calculations for this work, the whole composition of the alloys studied was taken into account.

SW Thermo-Calc (TC) has been developed as a complex heterogeneous system with highly non-ideal as well as ideal solution phases that can be applied to thermodynamic systems in the fields of chemistry, metallurgy, materials science, semiconductors, depending on the type of database used [27]. The software allows the use of several databases, where the TCFE database is mainly used for iron alloys. The work

Table 1 – Chemical composition of studied alloys (wt.%).

Alloy	C	Cr	Ni	O	P	S	Mn	Al	Cu	N
Ni1	0.382	0.010	1.084	0.002	0.004	0.006	0.030	0.010	0.014	0.003
Ni3	0.375	0.012	2.990	0.003	0.004	0.006	0.086	0.011	0.009	0.002
Ni5	0.338	0.010	4.478	0.001	0.005	0.006	0.031	0.011	0.012	0.003

reproduces the results obtained by SW Thermo-Calc version 2019a using the TCFE8 database. Elements H, P, and S were not included to avoid calculation instability.

3. Experimental

3.1. Sample characterization

The alloys were prepared from pure metals (Fe and Ni, purity 99.99%) and carbon (purity 99.99%) in a Leybold Heraeus furnace by vacuum induction melting and cast into a cylindrical mold without additional heat treatment.

Three model alloys based on Fe-C-Ni were studied. These alloys contained carbon between the range of 0.338–0.382 wt. % and nickel in the range of 1.084–4.478 wt. %. The chemical composition, determined by the GDA 750 HP optical emission spectrometer (GDOES), is listed in Table 1. In addition, the determination of carbon, oxygen, and sulfur contents was provided by Eltra 2000 CS and Eltra 2000 ONH combustion analyzers.

3.2. Differential thermal analysis (DTA) experiments

DTA measurements were performed to obtain temperatures of solidus (T_S), start ($T_{P,S}$) and end ($T_{P,E}$) of peritectic transformation and liquidus (T_L). The Setaram Setsys 18_{TM} device with S-type thermocouples was used for experimental measurements. The samples were measured in Al_2O_3 crucibles (100 μL), with an empty corundum crucible serving as a reference sample. The samples for DTA analysis were processed into a cylindrical form of diameter 3.5 mm, height 2.8 mm and mass of 190 ± 5 mg. Before analysis, they were polished to remove surface oxides and sonicated in acetone. All measurements were carried out under the same conditions in alumina crucibles at a heating rate of 10 °C·min^{-1}. Temperature calibration of DTA was performed using Pd (5N). The influence of the heating rate and sample mass was taken into account. An inert atmosphere of argon (purity higher than 99.9999%) was maintained during the experiments. Each alloy was measured three times, and therefore, the values in Table 2 correspond to the mean values.

3.3. Differential scanning calorimetry (DSC) experiments

The temperatures of phase transformations, heat capacity, enthalpy change, and heat of fusion were obtained by DSC method in a high-temperature area (above 1000 °C). The experimental measurements were performed using a Setaram MHTC 96 Line (Multi High-Temperature Calorimeter) with 3D heat-flux DSC sensor (B-type thermocouples). Samples for DSC analysis were processed into cylindrical form of diameter 5.0 mm, height 8.0 mm and mass of 1220 ± 5 mg. The alumina sleeves (volume 360 μL) were inserted into a platinum crucible and covered with an alumina cover and platinum cover. The whole set was then placed on the 3D DSC sensor and covered with the corundum cover. The empty corundum sleeve in the platinum crucible served as a reference sample. Measurements were carried out at a heating rate of 5 °C·min^{-1}.

Each alloy was measured once in two cycles, with Table 2 showing the average values. For temperature calibration, Pd (5N) was used, taking into account the influence of heating rate and sample mass. An inert atmosphere of helium instead of argon was used because helium has substantially higher thermal conductivity and, therefore, is more appropriate for measuring heat capacities [28]. The purity of the gas was higher than 99.9999%. Apparent heat capacities, heat capacities taking into account the impact of the latent heat of the phase transitions, were obtained by the continuous method.

The apparent heat capacities, which are the heat capacities considering the effect of the latent heat of phase transitions, were obtained by the continuous method.

Three measurements were carried out under the same experimental conditions. The first measurement was done with the empty corundum sleeves placed in Pt crucibles (blank), the second measurement with the reference sample Pt (3N5) and the last measurement with an alloy. Each alloy was subjected to two controlled cycling experiments (two heating and cooling cycles) under the same conditions.

The specific heat capacity of the sample is calculated according to equation (1) [29]:

$$C_p = C_{p,R}\frac{m_S.(A_s - A_b)}{m_R.(A_R - A_b)} \quad [J\cdot K^{-1}\cdot g^{-1}] \tag{1}$$

where

$C_{p,S}$ is specific heat capacity of the sample [J·K^{-1}·g^{-1}],
$C_{p,R}$ – specific heat capacity of the reference [J·K^{-1}·g^{-1}],
m_S – sample mass [g],
m_R – standard mass [g],
A_b – amplitude of the blank [μV],
A_R – amplitude of the standard [μV],
A_S – amplitude of the sample [μV].

From the experimentally obtained heat capacity and with use of Kirchhoff's law [30], enthalpy change was calculated. The heat of fusion was obtained in two ways. The heat of fusion was calculated from enthalpy change by extrapolation, which is shown in Fig. 1. There are several extrapolation options, which are listed, e.g., Ref. [31]. Furthermore, the heat of fusion was calculated from the DSC peak area.

3.4. Dilatometry experiments

The temperatures of phase transformations, coefficient of thermal expansion and density were determined by

dilatometry. A Netzsch DIL 402 Expedis Supreme NanoEye dilatometer with a S-type thermocouple was used for experimental measurements. The samples for dilatometric analysis were processed into cylinders with a diameter of 6.35 mm and a length of 10.05 mm. The mass of the cylinders was approximately 2400 mg. The samples were prepared to fill as much space as possible in the container with two pistons in which they were analyzed. Temperature calibration was performed using Pd (5N). Further, thermal expansion calibration was performed using the Al_2O_3 standard and correction to a sample holder. The measurements were carried out in sapphire containers (it was also included in the corrections). During the analysis, the dynamic atmosphere of helium was maintained in the furnace. The purity of helium was 99.9999%. Two measurements were carried out under the same experimental conditions, in Tables 2, 6 and 7 are listed mean values. The heating rate was 10 °C·min^{-1}. Throughout the experiment, a static force of 0.2 N was applied to the sample. The coefficient of thermal expansion was calculated as "technical alpha". The average coefficient of thermal expansion for the temperature interval $T_{ref} - T_1$ is mathematically defined as equation (2) [32]:

$$\alpha(T_1, T_{ref.}) = \frac{\frac{dL}{L_0}(T_1) - \frac{dL}{L_0}(T_{ref.})}{T_1 - T_{ref.}} \ [K^{-1}] \quad (2)$$

where.

L_0 is sample length measured at ambient temperature [mm],
T_1 – upper temperature limit [K],
$T_{ref.}$ – lower temperature limit named as reference temperature [K], in this case $T_{ref.} = 293{,}15$ K = 20 °C,
$\frac{dL}{L_0}$ – length change relative to L_0 [–].

Then the density for the T_1 temperature is calculated according to equation (3) [7]:

$$\rho(T_1) = \rho_{ref.}(T_{ref.}) \frac{\left(1 + \frac{dL}{L_0}(T_{ref.})\right)\left(1 + \alpha_{cont.}(T_{ref.})\right)^2}{\left(1 + \frac{dL}{L_0}(T_1)\right)\left(1 + \alpha_{cont.}(T_1)\right)^2} \ [g \cdot cm^{-3}] \quad (3)$$

where

$\rho_{ref.}$ is density of the solid at reference temperature,
$\alpha_{cont.}$ – tabulated coefficient of thermal expansion of the container material [K^{-1}].

4. Results and discussion

4.1. Temperatures of phase transformations

The phase transition temperatures were studied in the high-temperature area. Temperatures of solidus, liquidus, start, and end of peritectic transformation were detected by DTA, DSC method, and dilatometry. The experimental values were compared and discussed with theoretical calculations obtained by SWs IDS, JMatPro, and Thermo-Calc (Table 2). Fig. 2 shows all the DTA curves, and Fig. 3 shows all the dilatometric curves obtained for the analyzed alloys. Since DSC curves are very similar to DTA curves, they were not plotted.

Table 2 – Experimental and theoretical values of phase transition temperatures of studied alloys (°C).

°C	Experiment			Calculations		
	DTA	DSC	DIL	IDS	TC	JMP
Ni1						
T_S	1441	1445	1442	1437	1451	1439
$T_{P,S}$	1492	–	–	1496	1497	1500
$T_{P,E}$	1493	–	–	1497	1498	1501
T_L	1496	1502	1509	1502	1503	1502
Ni3						
T_S	1427	1436	1429	1430	1444	1435
T_L	1492	1500	1508	1497	1497	1499
Ni5						
T_S	1443	1445	1442	1431	1445	1440
T_L	1492	1499	1503	1496	1497	1499

As the nickel content increases, the liquidus temperature for DSC and dilatometric measurements decreases. For DTA measurements, the liquidus temperature is the same for Ni3 and Ni5 samples. The smallest temperature range in which melting takes place is for Ni5 alloy, and the largest is for Ni3 alloy.

It is clear from Fig. 2 that the Ni1 sample has the highest liquidus temperature and the Ni3 and Ni5 samples have a slightly lower T_L. The solidus temperature is almost identical to the Ni1 and Ni5 alloys, and for the Ni3 sample it is lower by 14–16 °C. The standard deviation for T_L determination was from 0 to 1 °C and for T_S was from 0 to 4 °C. The peritectic transformation was detected only for the Ni1 sample. It took place in the range of 1 °C. It follows that nickel narrows the area of peritectic transformation, which is also confirmed by the calculations performed by SW Thermo-Calc.

There is a very good agreement between the experimental and theoretical data for phase transformation temperatures. Differences are up to 14 °C, with a maximum for the Ni5 sample (T_S, DSC-IDS). Compared to individual SWs, the best agreement is between experimental and theoretical values with SW JMatPro. The standard deviation between the results of individual experimental methods ranges from 1 °C for sample Ni5 (T_S, DTA-DIL) to 7 °C for sample Ni3 (T_L, DTA-DIL).

The obtained experimental and theoretical results show that for the solidus temperature, the unambiguous influence of the change of the nickel content on its shift was not determined from the experimental results. This may also be due to the fact that it is challenging to correctly determine the solidus temperature, which is described in more detail in [14]. As the nickel content increased, the experimental and theoretical liquidus temperature decreased. The increase in nickel content in Fe-based alloys reduces the liquidus temperature according to [33–36] and the solidus temperature according to [33,37–39].

The results obtained from the statistical analysis show that the differences in the phase transformation temperatures in

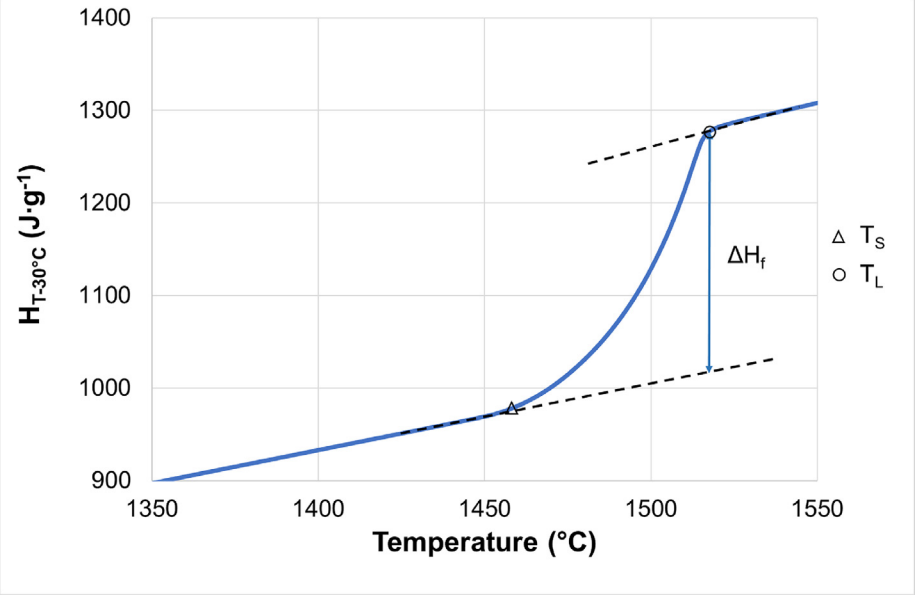

Fig. 1 – Temperature dependence of the enthalpy change in the melting range of the analyzed Ni1 sample with a graphical determination of the heat of fusion.

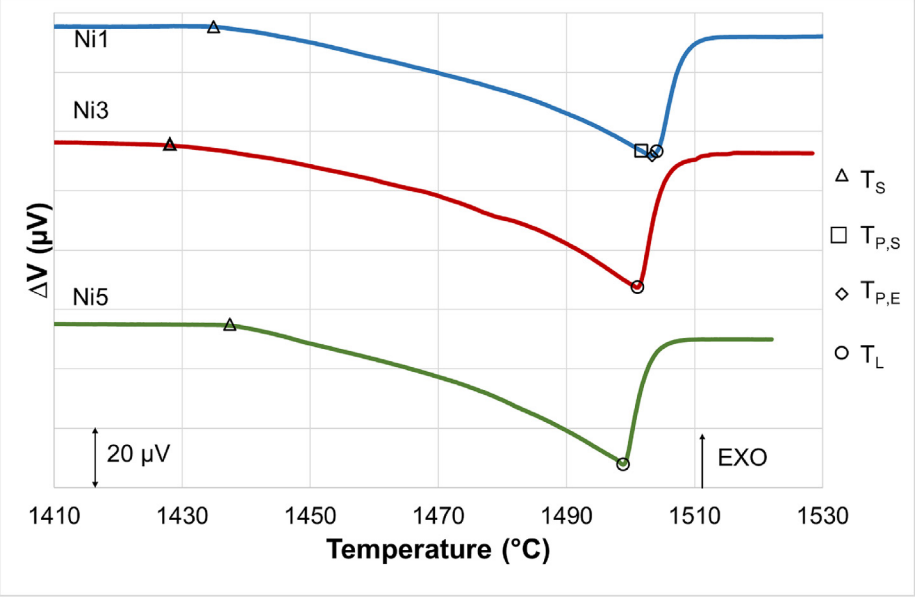

Fig. 2 – DTA curves of analyzed alloys.

comparison with individual experimental methods range from 1 to 16 °C. Concerning all methods used, the smallest deviation was obtained for the comparison of T_S (DTA-DIL), while the largest deviation was obtained for T_L (DTA-DIL). The differences may be due to the effects of the experimental conditions of the individual methods, the interactions of the individual elements, and the kinetics of the phase transformations.

4.2. *Heat capacity, enthalpy change and heat of fusion*

The heat capacities were studied in the temperature range of 1000–1575 °C by the 3D DSC method. According to Kirchhoff's equation, the numerical integration of this dependence gives the enthalpy as a function of temperature. The reference temperature for the calculation of enthalpy change was 30 °C. The heat of fusion was obtained in two ways, the first was the evaluation of the area of the DSC peak (ΔH_{DSC}), and the second was the evaluation of the enthalpy change (ΔH_E).

All experimental data were compared with theoretical calculations obtained by SWs JMatPro and Thermo-Calc, and the heat of solidification was also compared with SW IDS. Temperature dependencies of specific heat capacities are presented in Figs. 4–6, Table 3, enthalpy changes are presented in Fig. 7, Table 4 and experimental and theoretical values of heat of fusion are listed in Table 5.

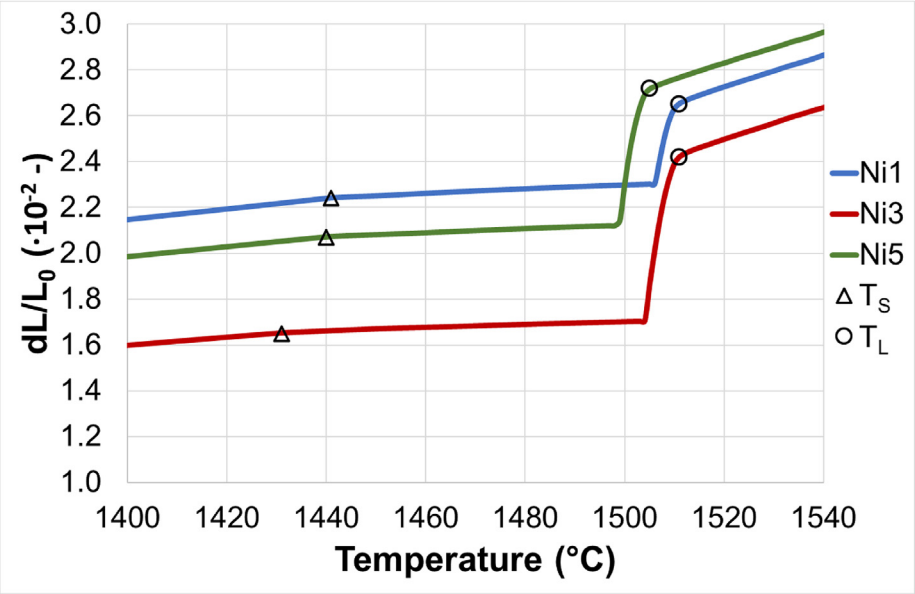

Fig. 3 – Dilatometric curves of analyzed alloys.

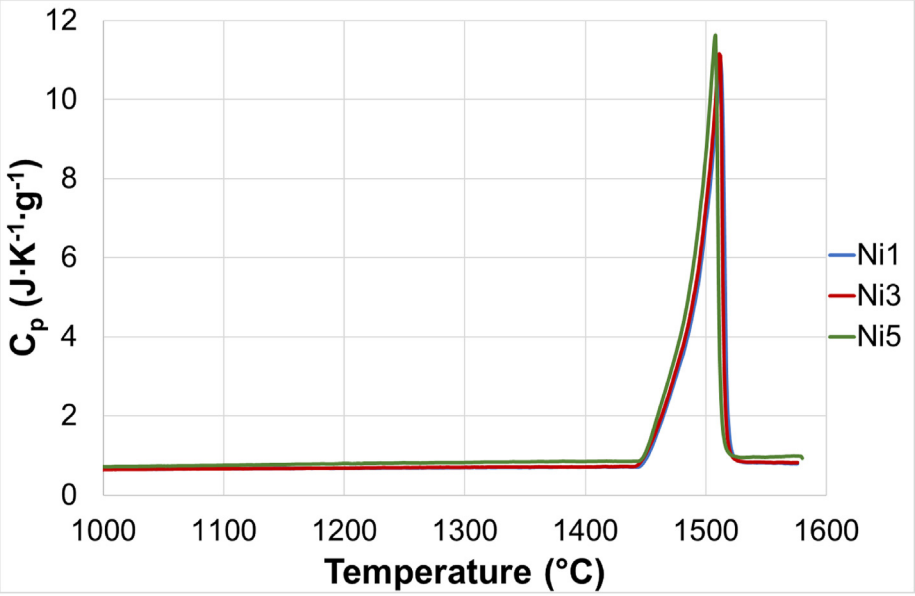

Fig. 4 – Temperature dependence of experimental specific heat capacities of analysed alloys.

In the temperature range 1000–1430 °C, the values of heat capacities of samples Ni1 and Ni3 are almost identical (C_p interval 0.64–0.73 $J \cdot K^{-1} \cdot g^{-1}$), with Ni5 alloy having higher values (C_p interval 0.72–0.86 $J \cdot K^{-1} \cdot g^{-1}$). If we compare the results calculated in SW JMatPro and Thermo-Calc in the temperature range 1000–1430 °C, both software show the same trends. With increasing nickel content, the values of heat capacities decrease, ranging from 0.62 to 0.70 $J \cdot K^{-1} \cdot g^{-1}$.

In the melting region, the maximum heat capacity value in T_L increases from 11.09 to 11.62 $J \cdot K^{-1} \cdot g^{-1}$ with increasing nickel content.

In the temperature range of 1530–1575 °C, the Ni1 and Ni3 samples have almost identical heat capacities, which are in the range of 0.80–0.84 $J \cdot K^{-1} \cdot g^{-1}$ and the Ni5 alloy has higher values ranging from 0.93 to 0.99 $J \cdot K^{-1} \cdot g^{-1}$. For the samples Ni1 and Ni3, a slight decrease in C_p is also visible up to 1560 °C, in the case of the sample Ni5 there is no decrease, and its values increase slightly over the whole interval. Heat capacities values should increase slightly in this area. The decrease in C_p values can be caused by the fact that in this temperature interval there are interactions associated with the melting process. Chemical heterogeneity causes that part of the sample is

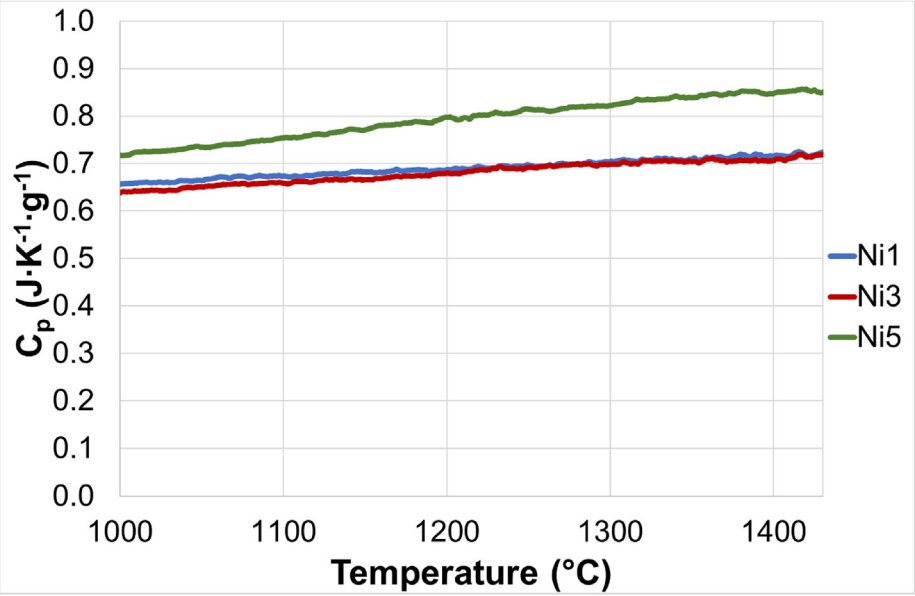

Fig. 5 – Temperature dependence of experimental specific heat capacities of analysed alloys, 1000–1430 °C.

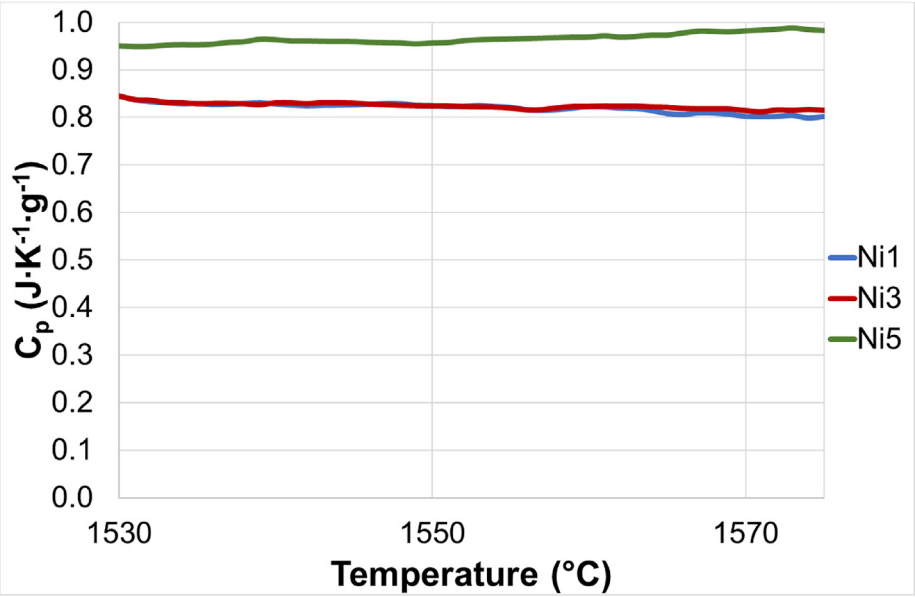

Fig. 6 – Temperature dependence of experimental specific heat capacities of analysed alloys, 1530–1575 °C.

not yet molten and there are clumps of solid particles in the sample. The experimental conditions may not yet be stabilized (transition from the heating zone to the isotherm). Difficult system control at high temperatures can also have an effect.

The same trends were observed from the comparison of SW JMatPro and Thermo-Calc in the temperature range of 1530–1575 °C. With increasing nickel content, heat capacities decrease, and their values are in the range of 0.82–0.83 J·K^{-1}·g^{-1}.

Statistical analysis using standard deviation showed that the smallest differences between experimental and theoretical values were for the Ni3 sample in the temperature range 1000–1430 °C (Exp-JMP, Exp-TC; value 0.02 J·K^{-1}·g^{-1}). The largest deviation was observed for the Ni3 sample in the melting range of 1431–1530 °C (Exp-JMP; value 3.88 J·K^{-1}·g^{-1}). The differences between the experimentally and theoretically obtained values of heat capacities can be caused by the fact that the calculations were performed under equilibrium conditions. The experimental results are influenced by the way

Table 3 – Experimental and theoretical values of specific heat capacities of studied alloys.

Temperature	Ni1			Ni3			Ni5		
	C_p			C_p			C_p		
	Exp	JMP	TC	Exp	JMP	TC	Exp	JMP	TC
(°C)	($J \cdot K^{-1} \cdot g^{-1}$)			($J \cdot K^{-1} \cdot g^{-1}$)			($J \cdot K^{-1} \cdot g^{-1}$)		
1000	0.66	0.63	0.63	0.64	0.63	0.63	0.72	0.63	0.62
1050	0.66	0.64	0.63	0.65	0.64	0.63	0.73	0.64	0.63
1100	0.67	0.65	0.64	0.66	0.64	0.64	0.75	0.64	0.64
1150	0.68	0.65	0.65	0.67	0.65	0.65	0.77	0.65	0.65
1200	0.69	0.66	0.66	0.68	0.66	0.66	0.80	0.66	0.66
1250	0.70	0.67	0.66	0.69	0.67	0.66	0.81	0.66	0.66
1300	0.71	0.68	0.67	0.70	0.68	0.67	0.82	0.67	0.67
1350	0.71	0.68	0.68	0.70	0.68	0.68	0.84	0.68	0.68
1400	0.72	0.69	0.69	0.71	0.69	0.69	0.85	0.69	0.69
1450	0.91	1.73	0.70	1.03	2.03	2.48	1.08	1.77	2.56
1500	6.93	13.73	8.03	7.31	0.81	0.81	8.63	0.81	0.81
1550	0.83	0.83	0.83	0.82	0.83	0.83	0.96	0.83	0.82

the samples are processed (mechanical and heat treatment), the experimental conditions, the kinetics of the course of phase transformations, and the dissolution of non-equilibrium phases.

For the alloys studied, it is not possible to determine a clear effect of the nickel content on the change in the heat capacity values from the experimental results. In almost the entire temperature range studied, the Ni1 and Ni3 alloys had identical or very close C_p values, unlike the Ni5 alloy, which had higher values. According to the calculations performed with SW JMat-Pro and Thermo-Calc in the temperature ranges of 1000–1430 °C and 1530–1580 °C, the heat capacities decrease with increasing nickel content. The values of the specific heat capacities of pure nickel in the temperature range from 1000 to 1575 °C according to [39] are from 0.59 to 0.73 $J \cdot K^{-1} \cdot g^{-1}$, and the values for pure iron according to the SW Thermo-Calc calculation are from 0.62 to 0.82 $J \cdot K^{-1} \cdot g^{-1}$. It implies that pure nickel has lower C_p values than pure Fe over the entire temperature range studied, so it should reduce C_p values in Fe–C–Ni based alloys.

Experimental values of enthalpy change ranged from 1000 to 1400 °C in the range of 633–963 $J \cdot g^{-1}$, during melting **(1400–1530 °C)** they ranged from 909 to 1338 $J \cdot g^{-1}$ and in the melt **(1530–1575 °C)** were in the range of 1269–1383 $J \cdot g^{-1}$, see Fig. 7 and Table 4. From 1000 to 1180 °C, the Ni1 sample has the highest ΔH values. The Ni5 sample has the highest ΔH values from 1180 °C up to the melt. Ni3 alloy has the lowest values from 1000 to 1575 °C. The heat of melting of ΔH_{DSC} wide range 292–312 J g^{-1}, while ΔH_E is in the range of 258–264 $J \cdot g^{-1}$,

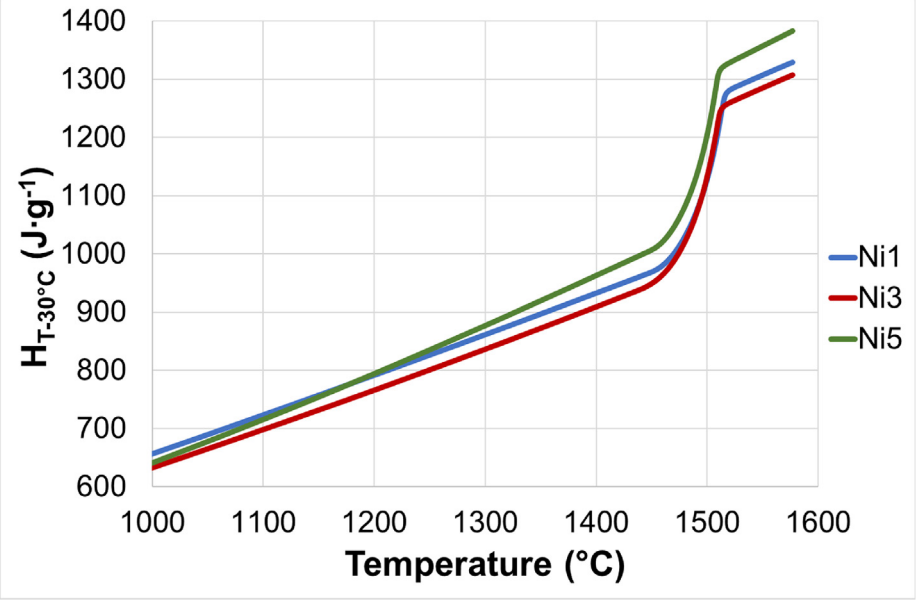

Fig. 7 – Temperature dependence of enthalpy change calculated from experimental C_p of analyzed alloys.

Table 4 – Experimental and theoretical values of enthalpy change of studied alloys.

Temperature	Ni1			Ni3			Ni5		
	$\Delta H_{T\text{-}30^{\circ}C}$			$\Delta H_{T\text{-}30^{\circ}C}$			$\Delta H_{T\text{-}30^{\circ}C}$		
	Exp	JMP	TC	Exp	JMP	TC	Exp	JMP	TC
(°C)	($J \cdot g^{-1}$)			($J \cdot g^{-1}$)			($J \cdot g^{-1}$)		
1000	657	686	688	633	682	684	641	679	680
1050	690	718	719	665	714	716	678	710	711
1100	724	750	751	698	746	748	715	742	743
1150	757	782	783	732	778	780	754	774	775
1200	792	815	816	766	811	813	794	807	808
1250	827	848	849	801	844	846	835	840	841
1300	862	881	882	836	878	879	877	873	874
1350	897	915	916	872	912	913	920	907	908
1400	933	950	950	909	946	947	963	941	942
1450	969	990	985	949	990	993	1007	982	986
1500	1129	1237	1248	1133	1269	1271	1204	1264	1266
1550	1308	1315	1316	1285	1310	1311	1357	1305	1306

Table 5 – Experimental and theoretical values of heat of fusion of studied alloys.

Sample	ΔH_{DSC}[a]			ΔH_E[b]	ΔH_{TC}	ΔH_{JMP}	ΔH_{IDS}
	($J \cdot g^{-1}$)						
Ni1	292	±	1	261	252	252	253
Ni3	293	±	1	258	246	257	252
Ni5	312	±	1	264	255	254	252

[a] Heat of fusion calculated from the DSC peak area.
[b] Heat of fusion calculated from the enthalpy change.

Table 5. The highest heat of phase transformation in both cases is for the Ni5 sample. The calculated values using the software are closer to the values calculated from the enthalpy change. This may be because when calibrating to the standard (Ni) from the peak area, the entire melting conversion may not be recorded, at the same time, the melting takes place in a very narrow temperature range, and the melting peak of the standard is different from the melting peak of Fe-based alloys.

The calculated values of the enthalpy change in the temperature range from 1000 to 1400 °C are from 679 to 950 $J \cdot g^{-1}$. Both of software calculated the same trends in the enthalpy change depending on the change in nickel content. The lowest values had the alloy Ni5 and the highest values had sample Ni1. As a result, the enthalpy change values decrease with increasing nickel content.

In the temperature range of 1400–1530 °C, the calculated values of the enthalpy change ranged from 943 to 1295 $J \cdot g^{-1}$. Calculations using both software showed the same trends. In the temperature ranges 1400–1450 °C and 1500–1530 °C, the Ni5 alloy had the lowest enthalpy change values and the highest values had Ni1 sample. In the temperature range 1451–1499 °C, the sample Ni1 had minimum values of enthalpy change and maximum values had Ni3 alloy.

The calculated values of the enthalpy change in the temperature range from 1530 to 1575 °C are from 1289 to 1338 $J \cdot g^{-1}$. Software calculations showed the same trends. Ni5 alloy had the lowest enthalpy change values and Ni1 alloy had the highest values. The effect of the change in nickel content was also confirmed in this area by decreasing the values of the change in enthalpy with increasing nickel content.

Statistical analysis using the standard deviation was evaluated. The best agreement between experimental and theoretical enthalpy change data was for Ni1 alloy in the temperature ranges 1000–1400 °C and 1530–1580 °C. The largest deviations were recorded for the Ni3 alloy (1000–1530 °C).

The experimental results show that the increasing nickel content does not have a clear effect on the enthalpy change. According to SWs JMatPro and Thermo-Calc calculations, increasing Ni content reduces enthalpy change values in the whole studied temperature range. The enthalpy change values for pure nickel are in the temperature range 1000–1575 °C according to [40] from 529 to 901 $J \cdot g^{-1}$. According to the SW Thermo-Calc calculations, pure iron has ΔH values from 674 to 1328 $J \cdot g^{-1}$ in the same study temperature interval. Based on this, the increasing nickel content in Fe–C–Ni based alloys should reduce the ΔH values in the whole studied temperature range.

The heat of fusion obtained from the DSC peak area increased with increasing nickel content. In the case of the heat of fusion obtained from the enthalpy change, an ambiguous trend was found for the studied alloys. From the results of the calculations of all SW products, the unambiguous effect of the change in nickel content on the shift of the heat of fusion values was not determined. The heat of fusion for pure nickel is 292 $J \cdot g^{-1}$ [41] and for pure iron is 247 $J \cdot g^{-1}$ (calculation in SW Thermo-Calc), so the heat of fusion of Fe–C–Ni based systems should increase with increasing nickel content.

From the methodological point of view and comparison of the results of two methods for the determination of heat of fusion, the method of determination from the enthalpy change appears more accurate.

The reason will probably be the method of enthalpic calibration used (calibration to the melting effect of the standard vs. calibration with Pt within the DSC method using the "continuous" method for obtaining C_p).

4.3. *Coefficient of thermal expansion and density*

The coefficient of thermal expansion and density were studied in the temperature range of 1000–1595 °C using dilatometry. All experimental data were compared with theoretical calculations obtained by SWs JMatPro and Thermo-Calc. Temperature dependence of coefficient of thermal expansion is presented in Fig. 8, Table 6 and density is presented in Fig. 9 and Table 7.

SWs JMatPro and Thermo-Calc do not calculate coefficient of thermal expansion directly in ver. 2019a, but the SWs calculate volume of the system and from this can be calculate volume coefficient of thermal expansion using a relation (4) [42]:

$$\beta = \frac{1}{V_0}\frac{dV}{dT} \quad [K^{-1}] \tag{4}$$

Coefficient of thermal expansion is calculated from volume coefficient of thermal expansion based on the assumption $\beta \approx 3\alpha$ [21,43].

In the temperature range of 1000 – 1400 °C are experimentally obtained values of coefficient of thermal expansion in the interval from 9.39 to $15.54 \cdot 10^{-6}$ K^{-1}. The lowest values of α are for alloy Ni3 and the highest for Ni1 alloy. Calculated values by both SWs were in the interval from 12.06 to $17.45 \cdot 10^{-6}$ K^{-1}. Calculations using both SWs had opposite trends of impact of nickel content change. According to SW JMatPro, the lowest values of α had Ni1 and the highest Ni5, which means that with increasing nickel content the values of the coefficient of thermal expansion increase. According to SW Thermo-Calc, the lowest values of the coefficient of thermal expansion had sample Ni5 and the highest values had Ni1 alloy, so with increasing nickel content the values of α decrease.

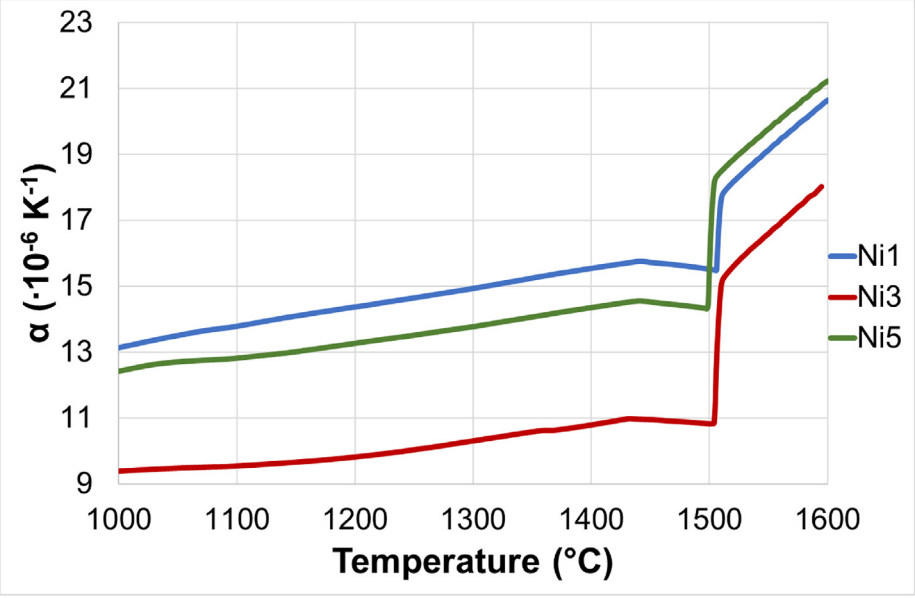

Fig. 8 – Temperature dependence of experimental coefficient of thermal expansion of analyzed alloys.

Table 6 – Experimental and theoretical values of coefficient of thermal expansion of studied alloys.

Temperature	Ni1			Ni3			Ni5		
	α			α			α		
	Exp	JMP	TC	Exp	JMP	TC	Exp	JMP	TC
(°C)	$\cdot 10^{-6}$ (K^{-1})			$\cdot 10^{-6}$ (K^{-1})			$\cdot 10^{-6}$ (K^{-1})		
1000	13.12	14.01	12.52	9.39	14.56	12.12	12.41	14.84	12.06
1050	13.49	14.49	12.98	9.48	15.01	12.58	12.70	15.28	12.51
1100	13.78	14.94	13.41	9.55	15.42	13.00	12.81	15.68	12.91
1150	14.09	15.35	13.81	9.66	15.81	13.38	13.01	16.05	13.29
1200	14.36	15.71	14.17	9.82	16.17	13.74	13.26	16.38	13.63
1250	14.64	16.05	14.51	10.04	16.49	14.07	13.51	16.68	13.95
1300	14.93	16.36	14.82	10.31	16.78	14.38	13.77	16.96	14.25
1350	15.24	16.66	15.12	10.58	17.04	14.66	14.06	17.21	14.53
1400	15.54	16.93	15.39	10.79	17.29	14.93	14.35	17.45	14.79
1450	15.72	17.46	15.65	10.95	17.91	15.73	14.52	17.91	15.49
1500	15.51	25.90	26.14	10.82	26.80	26.81	15.55	26.71	27.07
1550	19.13	27.27	27.11	16.59	27.32	27.07	19.77	27.24	27.34

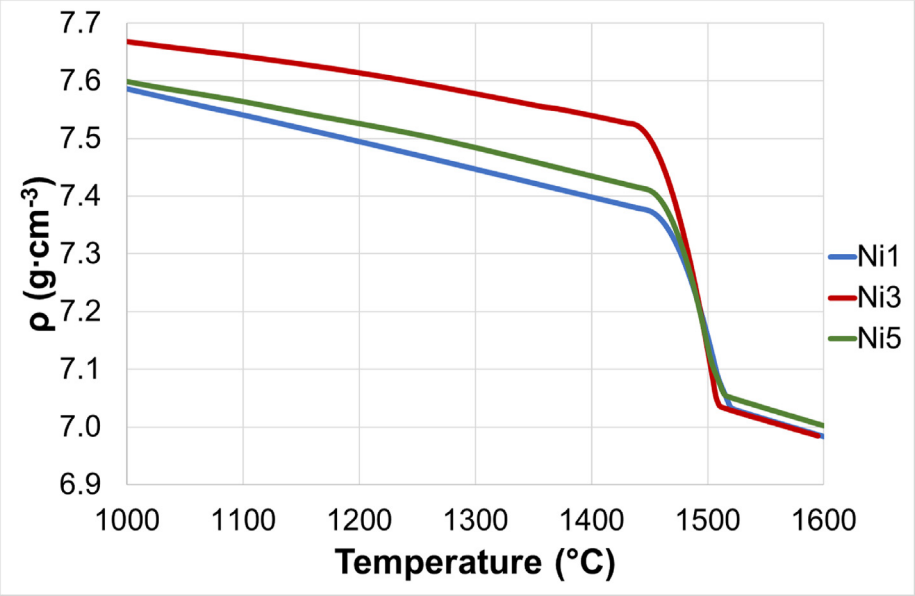

Fig. 9 – Temperature dependence experimental density of analyzed alloys.

In the melting range (1400–1530 °C) the experimental values of the coefficient of thermal expansion are in the range from 10.80 to 19.22·10^{-6} K^{-1}. In the temperature region 1400–1500 °C alloy Ni3 has the lowest values of α and sample Ni1 has the highest values of α. From 1501 to 1530 °C, the alloy Ni3 has the lowest values of the coefficient of thermal expansion and the highest has alloy Ni5. During melting, there is the largest increase in the coefficient of thermal expansion for the Ni3 sample and the smallest is for alloy Ni1. During melting (1400–1530 °C) the calculated values of the coefficient of thermal expansion are in the range from 14.80 to 27.23·10^{-6} K^{-1}. According to SW JMatPro, from 1400 to 1450 °C the alloy Ni1 has the lowest values of α and the highest has sample Ni5, from 1451 to 1502 °C the sample Ni1 has the lowest values of α, the highest has alloy Ni3 and from 1503 to 1530 °C it has the lowest values of α alloy Ni5 and the highest has sample Ni3. Calculations using SW Thermo-Calc have different trends due to changes in nickel content. From 1400 to 1450 °C, the alloy Ni5 has a minimum values of α and a maximum has sample Ni1, from 1451 to 1502 °C the sample Ni1 has the lowest values of α and the highest values has alloy Ni5, and from 1503 to 1530 °C has a minimum values of α alloy Ni3 and the highest Ni5. In the range of 1400–1450 °C according to the calculations of SW JMatPro with increasing nickel content the values of the coefficient of thermal expansion increase. Calculations according to SW Thermo-Calc show the opposite trend of the change of nickel content. For the temperature range 1451–1530 °C, it is not possible to determine a clear effect of the change in nickel content on the change in the values of the coefficient of thermal expansion.

In the liquid phase (1530–1595 °C) the experimental values of the coefficient of thermal expansion are from 15.98 to 21.10·10^{-6} K^{-1} Ni3 alloy has the lowest values and sample Ni5 has the highest values. In the temperature range 1530–1595 °C, the calculated values of the coefficient of thermal expansion are from 27.01 to 27.77·10^{-6} K^{-1}. According to SW JMatPro, the lowest values of α had Ni5 alloy and the highest had sample Ni3. According to the calculations of SW Thermo-Calc, the trend of the effect of the change of nickel content was the opposite, the lowest values of the coefficient of thermal expansion had the alloy Ni3 and the highest had sample Ni5.

Statistical analysis using the standard deviation was evaluated. The smallest difference between experimental and theoretical data was determined for alloy Ni1 (Exp-TC) in the temperature range of 1000–1400 °C. The highest standard deviation is for Ni3 alloy (Exp-JMP) in the temperature range 1531–1600 °C.

The largest differences between the experimental and theoretical values of the coefficient of thermal expansion are in the melting range (1401–1595 °C), which may be due to the fact that this area is substantially less studied, it is difficult to obtain experimental results from dilatometric measurements in the liquid phase (melting) and can also be caused by larger deviations in the input data of thermodynamic databases for the calculations.

The obtained results show that the increasing nickel content reduces the experimental values of the coefficient of thermal expansion in the whole studied temperature range. According to the results of SW JMatPro, the increasing nickel content increases the α values from 1000 to 1400 °C and according to SW Thermo-Calc it decreases them. From 1401 to 1595 °C, the unambiguous influence of nickel on the change in the values of the coefficient of thermal expansion was not demonstrated for both SWs. According to [41], the values of the coefficient of thermal expansion in the temperature range 1000–1342 °C are from 20.28 to 23.79·10^{-6} K^{-1}, for pure iron the values calculated in SW Thermo-Calc are in the same temperature range from 12.27 to 15.40·10^{-6} K^{-1}, at 1595 °C the α value is 27.48·10^{-6} K^{-1}. Based on this, it could be assumed

Table 7 – Experimental and theoretical values of density of studied alloys.

Temperature	Ni1			Ni3			Ni5		
	ρ			ρ			ρ		
	Exp	JMP	TC	Exp	JMP	TC	Exp	JMP	TC
(°C)	($g \cdot cm^{-3}$)			($g \cdot cm^{-3}$)			($g \cdot cm^{-3}$)		
1000	7.59	7.55	7.59	7.67	7.56	7.61	7.60	7.56	7.63
1050	7.56	7.53	7.57	7.65	7.53	7.58	7.58	7.54	7.60
1100	7.54	7.50	7.54	7.64	7.51	7.56	7.56	7.51	7.58
1150	7.52	7.48	7.52	7.63	7.48	7.54	7.54	7.49	7.56
1200	7.50	7.45	7.50	7.61	7.45	7.51	7.53	7.46	7.53
1250	7.47	7.43	7.47	7.60	7.43	7.49	7.51	7.44	7.51
1300	7.45	7.40	7.45	7.58	7.40	7.47	7.48	7.41	7.49
1350	7.42	7.37	7.42	7.56	7.38	7.44	7.46	7.39	7.47
1400	7.40	7.35	7.40	7.54	7.36	7.42	7.43	7.36	7.44
1450	7.37	7.32	7.38	7.50	7.32	7.38	7.41	7.33	7.41
1500	7.16	7.05	7.05	7.13	7.04	7.04	7.14	7.06	7.05
1550	7.01	6.99	7.00	7.01	7.00	7.01	7.03	7.02	7.02

that the increasing nickel content in Fe–C–Ni based alloys should increase the α values.

In the temperature range from 1000 to 1400 °C, the alloy Ni3 has the highest experimental density and the lowest has sample Ni1, range from 7.40 to 7.67 $g \cdot cm^{-3}$, see Fig. 9 and Table 7. The calculated density is in range from 7.35 to 7.63 $g \cdot cm^{-3}$. Calculations using both SWs have the same trends. Ni1 alloy has the lowest values of ρ and Ni5 the highest density. As a result, the density increases in this area with increasing nickel content.

In the temperature range 1400–1530 °C, the experimental values of density are in the range from 7.02 to 7.54 $g \cdot cm^{-3}$. From 1400 to 1509 °C, the sample Ni1 has the lowest values of ρ and the highest has alloy Ni3. In this temperature range, with increasing nickel content, the density increases, but again this is not a linear dependence. From 1510 to 1530 °C, Ni5 alloy has the lowest ρ values and alloys Ni1 (1510–1515 °C) and Ni3 (1516–1530 °C) have the highest values of density.

The calculated density values in the temperature range 1400–1530 °C are from 7.01 to 7.44 $g \cdot cm^{-3}$. According to SW JMatPro, in the temperature intervals 1400–1460 °C and 1502–1530 °C the alloy Ni1 has the lowest values of ρ and the highest has sample Ni5. This means that with increasing nickel content the density increases. From 1461 to 1501 °C, the sample Ni3 has the lowest values of ρ and the highest values has alloy Ni5. It is no longer possible to determine a clear dependence here. According to calculations by SW Thermo-Calc has Ni1 alloy in the temperature ranges 1400–1457 °C and 1502–1530 °C the lowest values of density and the highest values has sample Ni5 (with increasing nickel content the density increases). In the temperature range 1458–1501 °C the sample Ni3 has minimum values of ρ and maximum values have alloys Ni5 (1458–1497 °C) and Ni1 (1498–1501 °C).

In the liquid phase (1530–1595 °C) the experimental density values are in the range from 6.98 to 7.04 $g \cdot cm^{-3}$. Ni1 and Ni3 alloys have the same values of density, which are the lowest, the Ni5 sample has higher values of density. In this area, it is not possible to determine a clear trend of the impact of the change in nickel content on the change in ρ values. The calculated density values are in the range from 6.95 to 7.03 $g \cdot cm^{-3}$. Calculations using both software have the same trends. Ni1 alloy has the lowest values of ρ and Ni5 has the highest values of density. As a result, the density increases in this temperature range with increasing nickel content.

The standard deviation outside the phase transformations ranged from 0.00 to 0.30 $g \cdot cm^{-3}$ and in the phase transformations is from 0.01 to 0.28 $g \cdot cm^{-3}$. The best agreement was for Ni1 alloy (Exp-TC) in the temperature range

Table 8 – Influence of nickel on the change of studied properties.

	Exp	IDS	JMP	TC		
T_S	–	–	–	–		
T_L	↓	↓	↓	↓		
ΔH_{DSC}	↑	↓	–	–		
ΔH_E	–					

Temperature range (°C)	Heat capacity			Enthalpy change		
	Exp	JMP	TC	Exp	JMP	TC
1000–1400	–	↓	↓	–	↓	↓
1401–1530	–			–	↓	↓
1531–1575	–	↓	↓	–	↓	↓

Temperature range (°C)	Coefficient of thermal expansion			Density		
	Exp	JMP	TC	Exp	JMP	TC
1000–1400	↓	↑	↓	↑	↑	↑
1401–1530	↓	–	–	↑	↑	↑
1531–1595	↓	–	–	–	↑	↑

↑ With increasing nickel content the values of the observed property increase.
↓ With increasing nickel content the values of the observed property decrease.
- It was not possible to unambiguously determine the effect of nickel on the change in the values of the observed property.

1000–1400 °C. The most significant deviations were recorded during melting for the Ni3 sample for both SWs.

The experimental results show that in the temperature range 1000–1509 °C the alloy Ni1 has the minimum values of ρ and maximum values has alloy Ni3 or Ni5. In this temperature range, the increasing nickel content probably increases the density. According to SW JMatPro calculations, the growing nickel content increases the density in almost the entire studied temperature range, except for 1461–1501 °C. SW Thermo-Calc calculations have the same trend. According to [41], the density values for pure nickel in the temperature range 1000–1595 °C are from 7.73 to 8.46 $g \cdot cm^{-3}$. According to the SW Thermo-Calc calculations for pure iron in the same temperature range, the density is from 6.97 to 7.60 $g \cdot cm^{-3}$. It follows that the increasing nickel content in Fe–C–Ni based alloys should increase the density values.

Obtaining the correct dilatometric data in the melting region of materials is experimentally challenging and expensive. Experimental results can be affected by sample shrinkage during melting, rod deformation at higher temperatures, and scrubbing of the pistons in the container. Apart from the mentioned, there is also a scarcity of literature data. For these reasons, the dilatometric experimental results are very valuable.

5. Conclusions

Original data concerning temperatures of phase transformations during melting, specific heat capacity, enthalpy change, heat of fusion, coefficient of thermal expansion, and density for three model alloys based on Fe–C–Ni were obtained not only experimentally by DTA, DSC, and dilatometry, but also theoretically by SW JMatPro, Thermo-Calc and for the phase transformation temperatures and heat of fusion by SW IDS. The effect of nickel on the change in the properties obtained is listed in Table 8.

Based on the obtained results, the following conclusions can be stated:

5.1. *In the case of the temperatures of phase transformations*

- For the experimental and theoretical values of solidus temperature, an unambiguous influence of changing the nickel content on their shift was not found. Research according to [33,37–39] and calculations show that increasing the nickel content should reduce T_S values.
- The experimental and theoretical liquidus temperature decreased with increasing nickel content, which is in line with the current state of knowledge.

5.2. *In the case of heat capacity, enthalpy change, and heat of fusion*

- A clear effect of the change in the nickel content on the shift of C_p values was not detected from the experimentally obtained values. According to the literature [40], SWs JMatPro and Thermo-Calc calculations, the heat capacities decrease with increasing nickel content.
- Concerning experimental values of enthalpy change, a clear effect of nickel content was not detected. According to research [40], SWs JMatPro and Thermo-Calc calculations, the increase in the nickel content reduces enthalpy change values in the whole studied temperature range.
- The heat of fusion obtained from the DSC peak area increased with increasing nickel content, which is correlated with the results reported in [41]. For the heat of fusion obtained from enthalpy change, no clear effect of the nickel content on its change was detected. The same applies to all theoretical results.

5.3. *In the case of coefficient of thermal expansion and density*

- With increasing nickel content, the experimental values of thermal expansion coefficient decreased in the whole studied temperature range. According to the results presented in [41] and SW JMatPro, a higher nickel content increases the α values from 1000 to 1400 °C but decreases them according to SW Thermo-Calc. From 1401 to 1595 °C, the unambiguous influence of nickel on the change in the values of the coefficient of thermal expansion was not demonstrated for both SWs.
- In the temperature range of 1000–1509 °C, the nickel content increases the experimental density values. The same trend was observed using SWs JMatPro, Thermo-Calc and theoretical research [44]. The results show that even for relatively simple systems (alloys), there are significant differences between experimental and theoretical values.

The high quality of experimental material data of these systems (Fe–C and Fe–C–Ni) is crucial for a better understanding of more complex or even polycomponent systems (especially steels and related alloys). In some cases, significant differences between experimental and theoretical results may be due, among other things, to the fact that the calculations are performed in equilibrium while the experiment is only approaching it. Another reason may be the lack of accurate experimental data for calculations and incomplete databases for calculations, also the experimental method and methodology used, and the demanding experimental acquisition of some properties, e.g., accurate determination of solidus temperature or results of studied properties (C_p, ΔH, α, ρ) in the melt.

The acquired knowledge is valuable regarding the current issues in the field of solidification, segregation, welding, heat treatment, structure optimization, mechanical properties, phase equilibrium, kinetics, and many others. The data obtained can be used as input data for numerical models simulating the crystallization, solidification, and cooling of metal castings with similar chemical compositions. They can contribute to the improvement and supplementation of software databases (SW FactSage and Thermo-Calc) and the improvement of technological processes by means of simulations, e.g., in SW Procast and Magmasoft. The simulation results can subsequently help to increase homogeneity and reduce casting errors.

Declaration of Competing Interest

The authors declare that they have no known competing financial interests or personal relationships that could have appeared to influence the work reported in this paper.

Acknowledgements

This paper was created within the frame of the project No. CZ.02.1.01/0.0/0.0/17_049/0008399 from the EU and CR financial funds provided by the Operational Programme Research, Development and Education, Call 02_17_049 Long-Term Intersectoral Cooperation for ITI, Managing Authority: Czech Republic - Ministry of Education, Youth and Sports, and student project SP2022/39.

REFERENCES

[1] Berns H, Theisen W. Ferrous materials: steel and cast iron. Heidelberg: Springer Berlin; 2008.
[2] Smil V. Still the iron age. Oxford: Butterworth-Heinemann; 2016.
[3] Rana R, editor. High-performance ferrous alloys. Cham: Springer; 2021.
[4] Harvey LDD. Iron and steel recycling: review, conceptual model, irreducible mining requirements, and energy implications. Renew Sustain Energy Rev 2021;138:110553.
[5] Mitra A. Use of steel as a sustainable concept. In: Hashmi S, Choudhury IA, editors. Encyclopedia of renewable and sustainable materials. vol. 4. Amsterdam: Elsevier; 2020. p. 315–29.
[6] Sun W, Wang Q, Zhou Y, Wu Y. Material and energy flows of the iron and steel industry: status quo, challenges and perspectives. Appl Energy 2020;268:114946.
[7] Sun J, Na H, Yan T, Qiu Z, Yuan Y, He J, et al. A comprehensive assessment on material, exergy and emission networks for the integrated iron and steel industry. Energy 2021;235:121429.
[8] Miettinen J. Calculation of solidification-related thermophysical properties for steels. Metall Mater Trans 1997;28(2):281–97.
[9] Levykina AG, Shkatov VV, Mazur IP. Hot rolling strips at the casting and rolling unit during coil-to-coil and endless rolling modes. Procedia Manuf 2019;37:472–7.
[10] Gur CH, Pan J, editors. Handbook of thermal process modeling steels. 1st ed. Boca Raton: CRC Press; 2008.
[11] Xu T, Song G, Yang Y, Ge P-X, Tang L-X. Visualization and simulation of steel metallurgy processes. Int. J. Miner. Metall. Mater. 2021;28:1387–96.
[12] Haines PJ, Reading M, Wilburn FW. Differential thermal analysis and differential scanning calorimetry. In: Brown ME, editor. Handbook of thermal analysis and calorimetry. vol. 1. Amsterdam: Elsevier Science B.V; 1998. p. 279–361.
[13] Boettinger WJ, Kattner UR, Moon K-W, Perepezko JH. DTA and heat flux DSC measurements of alloy melting and freezing. In: Zhao J-C, editor. Methods for phase diagram determination. Amsterdam: Elsevier Science Ltd; 2007. p. 151–221.
[14] Drozdová Ľ, Smetana B, Presoly P, Novák V, Machů M, Bernhard M, et al. Investigation of Fe–C–Cr and Fe–C–Cr–Ni-based systems with the use of DTA and HT-LSCM methods. J Therm Anal Calorim 2020;142(2):535–46.
[15] Moon S-C, Phelan D, Dippenaar R. New insights of the peritectic phase transition in steel through in-situ measurement of thermal response in a high-temperature confocal microscope. Mater Char 2021;172:110841.
[16] Fukuyama H, Higashi H, Yamano H. Effect of B4C addition on the solidus and liquidus temperatures, density and surface tension of type 316 austenitic stainless steel in the liquid state. J Nucl Mater 2021;554:153100.
[17] Jung IH, Van Ende MA. Computational thermodynamic calculations: FactSage from CALPHAD thermodynamic database to virtual process simulation. Metall Mater Trans 2020;51:1851–74.
[18] Zhang Y, Yang J. CALPHAD-based alloy design of cast austenitic heat-resistant steels with enhanced strength at 1000 °C. Calphad 2019;67:101679.
[19] Liu W, Chen C, Tang Y, Long Q, Wei S, Zhang G, et al. Thermodynamic evaluation and investigation of solidification microstructure in the Fe–Cr–Ni–C system. Calphad 2020;69:101763.
[20] Khvan AV, Hallstedt B, Broeckmann C. A thermodynamic evaluation of the Fe–Cr–C system. Calphad 2014;46:24–33.
[21] Hillert M, Qiu C. A thermodynamic assessment of the Fe-Cr-Ni-C system. Metall Mater Trans 1991;22:2187–98.
[22] Ahssi MAM, Erden MA, Acarer M, Çuğ H. The effect of nickel on the microstructure, mechanical properties and corrosion properties of Niobium-Vanadium Microalloyed Powder metallurgy steels. Materials 2020;13(18):4021.
[23] Carvill J. Engineering materials. In: Carvill J, editor. Mechanical engineer's data handbook. Butterworth-Heinemann; 1993. p. 218–66.
[24] Papavinasam S. Materials. In: Papavinasam S, editor. Corrosion control in the oil and gas industry. Gulf Professional Publishing; 2014. p. 133–77.
[25] Miettinen J, Louhenkilpi S, Kytönen H, Laine JIDS. Thermodynamic–kinetic–empirical tool for modelling of solidification, microstructure and material properties. Math Comput Simulat 2010;80(7):1536–50.
[26] Saunders N, Guo UKZ, Li X, Miodownik AP, Schillé J-S. Using JMatPro to model materials properties and behavior. J Occup Med 2003;55:60–5.
[27] Andersson JO, Helander T, Hoglund L, Hi Pa, Sundman B. Thermo-Calc & DICTRA, computational tools for materials science. Calphad 2002;26(2):273–312.
[28] Luisi M, Wilthan B, Pottlacher G. Influence of purge gas and spacers on uncertainty of high-temperature heat flux DSC measurements. J Therm Anal Calorim 2015;119:2329–34.
[29] Zhao G, Wang R, Liu S, Wang T, Wu D, Zhang Y, et al. Microstructure analysis of element W in improving the Ni–P deposit thermal stability. J Mater Res Technol 2020;9(3):5474–86.
[30] Atkins PW. Physical chemistry. 10th ed. Oxford: Oxford University Press; 2016.
[31] Kalup A, Smetana B, Kawuloková M, Zlá S, Francová H, Dostál P, et al. Liquidus and solidus temperatures and latent heats of melting of steels. J Therm Anal Calorim 2017;127(1):123–8.
[32] Koniorczyk P, Zmywarczyk J, Debski A, Zielinski M, Preiskorn M, Sienkiewicz J. Investigation of thermophysical properties of three Barrel steels. Metals 2020;10(5):573.
[33] Cabrera-Marrero JM, Carreno-Galindo V, Morales RD, Chaves-Alcala F. Macro-Micro modeling of the dentritic microstructure of steel billets processes by continuous casting. ISIJ Int 1998;38(8):812–21.
[34] Han Z, Cai K, Liu B. Prediction and analysis on formation of Internal Cracks in. ISIJ Int 2001;41(12):1473–80. 2001.
[35] Diederichs R, Bleck W. Modelling of Manganese Sulphide formation during solidification, Part I: Description of MnS formation Parameters. Steel Res Int 2006;77(3):202–9.

[36] Diederichs R, Bülte R, Pariser G, Bleck W. Modelling of Manganese Sulphide formation during solidification, Part II: Correlation of solidification and MnS formation. Steel Res Int 2006;77:256–64.
[37] Štětina J Kavička F. The influence of the chemical composition of steels on the numerical simulation of a continuously cast slab. Materiali in Tehnologije 2011;45(4):363–7.
[38] Han ZB, Liu JH, Ha Y, Li KW, Ji YL, Liu J. Determination of the liquidus and solidus temperatures of FeCrAl stainless steel. IJMMM 2015;22(11):1141–8. 2015.
[39] Fruehan RJ. The making, shaping, and treating of steel. 11th ed. Pittsburg: AISE Steel Foundation; 1998.
[40] Desai PD. Thermodynamic properties of nickel. Int J Thermophys 1987;8(6):763–80.
[41] Quested PN. Valencia JJ. Thermophysical properties. In: Furrer D, Semiatin SL, editors. Metals process simulation. ASM handbook, 22B. ASM; 2010. p. 18–32.
[42] Callister WD. Materials science and engineering: an introduction. 10th ed. Hoboken: Wiley; 2020.
[43] Al-Rubaie KS, Pohl M. Heat treatment and two-body abrasion of Ni-Hard 4. Wear 2014;312(1–2):21–8.
[44] Abdullaev RN, Kozlovskii YM, Khairulin RA, Stankus SV. Density and thermal expansion of high purity nickel over the temperature range from 150 K to 2030 K. Int J Thermophys 2015;36:603–19.